

## RESEARCH ARTICLE

 OPEN ACCESS

Received: 05.11.2020

Accepted: 04.02.2021

Published: 08.02.2021

**Citation:** Prasad K, Reddy GR, Raju BDP (2021) Surfactant assisted morphological transformation of rod-like  $\text{ZnCo}_2\text{O}_4$  into hexagonal-like structures for high-performance supercapacitors. Indian Journal of Science and Technology 14(7): 676-689. <https://doi.org/10.17485/IJST/v14i7.2002>

## \* Corresponding author.

Tel: +91-9440281769  
[drdevaprasadraju@gmail.com](mailto:drdevaprasadraju@gmail.com)

**Funding:** Rajiv Gandhi National Fellowship (RGNF)

**Competing Interests:** None

**Copyright:** © 2021 Prasad et al. This is an open access article distributed under the terms of the [Creative Commons Attribution License](https://creativecommons.org/licenses/by/4.0/), which permits unrestricted use, distribution, and reproduction in any medium, provided the original author and source are credited.

Published By Indian Society for Education and Environment ([iSee](https://www.indjst.org/))

## ISSN

Print: 0974-6846

Electronic: 0974-5645

# Surfactant assisted morphological transformation of rod-like $\text{ZnCo}_2\text{O}_4$ into hexagonal-like structures for high-performance supercapacitors

**Kumcham Prasad<sup>1</sup>, Gutturu Rajasekhara Reddy<sup>1</sup>, Borelli Deva Prasad Raju<sup>2\*</sup>**<sup>1</sup> Department of Instrumentation, Sri Venkateswara University, Tirupati, 517502, India<sup>2</sup> Department of Physics, Sri Venkateswara University, Tirupati, 517502, India. Tel.: +91-9440281769

## Abstract

**Objectives:** To develop the microstructures of rod-shaped  $\text{ZnCo}_2\text{O}_4$  (ZCO-Urea) and hexagonal-shaped  $\text{ZnCo}_2\text{O}_4$  (ZCO- $\text{NH}_4\text{F}$ ) through the change of surfactants such as urea and  $\text{NH}_4\text{F}$  in the reaction and to investigate the physicochemical and electrochemical properties for high-performance supercapacitors. **Methods:** The structural and morphological characteristics of two prepared samples were analyzed through X-ray diffraction analysis (XRD), Scanning electron microscope (SEM) analysis, and Transmission electron microscope (TEM) analysis, respectively. The electrochemical performance was evaluated using Cyclic voltammetry (CV), Galvanostatic charge-discharge (GCD), and Electrochemical impedance spectroscopy (EIS) analysis. **Findings:** The crystalline nature and phase purity of the as prepared samples were confirmed from XRD, and the structural parameters such as lattice parameter ( $a$ ), microstrain ( $\epsilon$ ), dislocation density ( $\delta$ ), cell volume ( $v$ ), and average crystalline size ( $D$ ) for both the samples were determined. The SEM and TEM analysis revealed morphological characteristics of the samples. The electrochemical analysis of ZCO-Urea and ZCO- $\text{NH}_4\text{F}$  electrodes were tested for supercapacitor application in 1M of aqueous KOH electrolyte and exhibit an areal capacitance of  $31 \text{ mF cm}^{-2}$ , and  $41.43 \text{ mF cm}^{-2}$ , respectively, obtained at a current density of  $10 \mu\text{A cm}^{-2}$ . And also showed outstanding cyclic stability over 1000 charge-discharge cycles. **Applications:** The simple and inexpensive method of synthesized surfactant-assisted morphological transformation of ZCO microstructures will introduce new directions in this emerging energy field.

**Keywords:**  $\text{ZnCo}_2\text{O}_4$ ; Urea;  $\text{NH}_4\text{F}$ ; areal capacitance; supercapacitors

## 1 Introduction

As the non-renewable energy resources such as fossil fuels become rarer and the increasing demand for energy to meet current energy requirements leads to an intense search for alternative energy sources and the use of energy devices. This is further

stressed by the rapid increment in possession of consumer electronic goods and portable devices<sup>(1–4)</sup>. In this scenario, supercapacitors (SCs) are studied as one of the best-suited technologies for energy storage devices due to their longer cycle life, higher power density, faster charging-discharging ability, smaller size, and safe operation, and eco-friendly characteristics than many other energy storage devices. Apart from the advantages of SCs, the successful exploitation of renewable energy resources still requires more efficient, low-cost, reliable, and eco-friendly characteristics<sup>(5,6)</sup>.

SCs can be generally sorted in terms of their charge storage mechanism into two classes as electric double-layer capacitors (EDLCs) in which the charge is stored due to non-faradaic reversible ion adsorption at the electrode/electrolyte's interface. Still, it is achieved for pseudocapacitors (PCs) due to the reversible faradaic redox reactions of the active electrode material<sup>(7)</sup>. Since the electrode material is one of the significant components in enhancing the energy storage device's electrochemical performance, novel materials and materials with varying morphological characteristics have been investigated. Carbonaceous materials, conducting polymers, and transition metal oxides (TMOs) are the various types of most commonly used electrode materials. The latter was widely explored for PCs due to their high theoretical capacitance and abundant oxidation states. The PCs exhibit higher charge storage ability than EDLCs, but their usage is still rendered by their high cost and poor cycling stability. The electrochemical performance of PCs mainly depending on the size, morphology, architecture of the electroactive material and can be enhanced by using nanostructured materials<sup>(8)</sup>.

In this view, most of the current research work has been focussed on the rational design of porous structures, novel heterostructures, and hierarchical architectures of the electrode materials using various strategies like introducing structure-directing agents, ligands to synthesize more effective electroactive materials with special structures<sup>(9,10)</sup>. Among the TMOs, the AB<sub>2</sub>O<sub>4</sub> type binary transition metal oxides (BTMOs) like NiCo<sub>2</sub>O<sub>4</sub><sup>(11)</sup>, MnCo<sub>2</sub>O<sub>4</sub><sup>(12)</sup>, ZnCo<sub>2</sub>O<sub>4</sub><sup>(13)</sup>, CuCo<sub>2</sub>O<sub>4</sub><sup>(14)</sup>, and ZnFe<sub>2</sub>O<sub>4</sub><sup>(15)</sup> are the most explored electrode materials for supercapacitors than their corresponding single-component metal oxides due to the advantages like rich redox chemistry, combined contributions of both the metal ions, etc. ZnCo<sub>2</sub>O<sub>4</sub>, as one of the most promising BTMOs, has been widely explored as active electrode material for energy storage applications like supercapacitors. This is due to its advantages like high theoretical specific capacitance, variable oxidation states, low-cost, environmental-friendly characteristics, and easy availability. Further, both zinc and cobalt cations' contributions offer a synergetic effect on the redox chemistry of ZnCo<sub>2</sub>O<sub>4</sub> electrode material. This is due to the Co ions' high capacitance and the greater number of electron transportation channels provided by the Zn ions<sup>(16,17)</sup>. A wide range of micro/nanostructures of ZnCo<sub>2</sub>O<sub>4</sub> were synthesized through different methods to date<sup>(18–20)</sup>.

The morphology of the ZnCo<sub>2</sub>O<sub>4</sub> depends on mainly the reaction or experiment parameters such as reaction time and temperature, solvent and surfactant type, and precursors concentration. In our previous reported papers, different types of morphologies were synthesized by adjusting the synthesis parameters and investigated the physicochemical, textural and electrochemical properties for supercapacitors in terms of specific capacitance (F/g). The novelty of the present work involves, to prepare two different morphologies by varying the surfactant in the hydrothermal reaction and other synthesis conditions are the same. Hexagonal and rod-like morphologies were obtained and exhibits different electrochemical performance for supercapacitors in terms of areal capacitance. Furthermore, the prepared two electrodes exhibit outstanding cyclic performance over 1000 cycles<sup>(21–23)</sup>

Despite these developments, there is still room for improving the morphological structures, which have a significant character in enhancing a device's energy storage ability, using low-cost materials and more straightforward synthesis methods. In this regard, researchers have focused on varying the material's morphological properties and controlling the size by using materials as surfactants and precipitants<sup>(24–28)</sup>. Herein we proposed a work focussed on tuning the morphology of ZnCo<sub>2</sub>O<sub>4</sub> (ZCO) material by varying surfactants like Urea and Ammonium fluoride using the hydrothermal method and represented as ZCO-Urea and ZCO-NH<sub>4</sub>F, respectively, throughout the study. The as-prepared materials are systematically studied using various physicochemical and electrochemical techniques. These results ensure that as-prepared materials are potential candidates for supercapacitors applications.

## 2 Materials and Methods

### 2.1 Materials

Zinc nitrate hexa-hydrate [Zn(NO<sub>3</sub>)<sub>2</sub>·6H<sub>2</sub>O], cobalt nitrate hexa-hydrate [Co(NO<sub>3</sub>)<sub>2</sub>·6H<sub>2</sub>O], urea [Co(NH<sub>2</sub>)<sub>2</sub>], ammonium fluoride (NH<sub>4</sub>F), ethanol (C<sub>2</sub>H<sub>5</sub>OH) and potassium hydroxide (KOH) were purchased from Sigma-Aldrich (India). All the chemicals above mentioned were AR grade and directly used after purchase. The solvent used is DI water with a resistivity of 18.2 MΩ cm for all the experiments.

## 2.2 Synthesis of rod/hexagonal-like ZnCo<sub>2</sub>O<sub>4</sub>

In a typical synthesis procedure, for rod-like ZnCo<sub>2</sub>O<sub>4</sub> (ZCO-Urea) 10 mmol of Zn (NO<sub>3</sub>)<sub>2</sub>·6H<sub>2</sub>O, 20 mmol of Co (NO<sub>3</sub>)<sub>2</sub>·6H<sub>2</sub>O, and 1 g of [CO(NH<sub>2</sub>)<sub>2</sub>] was dissolved in 35 ml of DI water and thoroughly stirred for 10 minutes. The obtained homogeneous clear solution was then transferred into a Teflon-lined stainless-steel autoclave of 50 mL volume and heated up to 180°C at a ramping rate of 2 °C/min and maintained at that temperature for 12 hours and allowed to cool down naturally to room temperature. After the reaction was over, the precipitate is collected and subjected to washing with DI water followed by absolute ethanol several times to remove the residual nanoparticle debris and allowed to dry at 80°C for 12 hours. Finally, the powder samples obtained are annealed at 400°C for 3 hours at a ramping rate of 2°C/min resulting in the formation of rod-like ZnCo<sub>2</sub>O<sub>4</sub> nanostructures. The synthesis procedure for hexagonal-like ZnCo<sub>2</sub>O<sub>4</sub> (ZCO-NH<sub>4</sub>F) was similar to rod-like ZnCo<sub>2</sub>O<sub>4</sub> (ZCO-Urea), except CO(NH<sub>2</sub>)<sub>2</sub> is replaced by NH<sub>4</sub>F.

## 2.3 Materials characterization

The crystalline nature and phase purity of the as prepared ZCO samples was determined using X-ray diffraction (XRD) analysis with a diffractometer (PANalytical X'Pert PRO, Malvern, UK) facilitated with Cu K<sub>α</sub> ( $\lambda = 1.5405980 \text{ \AA}$ ) as the radiation source, functioning voltage of 40 kV and a current of 30 mA within a  $2\theta$  range of 10–80° with a step size of 0.02°. The morphological characteristics were analyzed with a scanning electron microscope (SEM) (Model number FE-SEM, S-4800, Hitachi, Japan). During SEM measurements, an ultra-thin layer of Pt was sputter-coated (E-1030 Ion Sputter, Hitachi, Japan) onto the samples to increase the conductivity. The microstructures were examined using a transmission electron microscope (TEM) (HRTEM, Tecnai G2 F20 S-Twin, Hillsboro, USA). The electrochemical measurements of the samples were carried out on an electrochemical workstation (CHI 760E, CH instruments, USA) using a three-electrode system with 1 M KOH aqueous solution as the electrolyte at room temperature. A platinum wire was used as the counter electrode, Ag/AgCl acted as the reference electrode, and the as-prepared ZnCo<sub>2</sub>O<sub>4</sub> was used as the working electrode for all the measurements. The cyclic voltammetry (CV), galvanostatic charge-discharge (GCD) and electrochemical impedance spectroscopy (EIS) measurements were carried out to evaluate the electrochemical performance of the ZCO samples.

## 2.4 GCE preparation

For conducting the electrochemical measurements, a homogeneous suspension of 4 mg of active material in 2 mL of ethanol was prepared and 10  $\mu\text{L}$  of the resulting suspension was uniformly deposited on the glassy carbon electrode over an area of 0.06 cm<sup>2</sup>. The electrode had been dried under an infrared lamp and then washed thoroughly with de-ionized water before conducting the electrochemical measurements.

# 3 Results and discussion

## 3.1 X-ray diffraction analysis

The crystallinity of the as-prepared ZnCo<sub>2</sub>O<sub>4</sub> microstructures was studied by XRD analysis. The characteristic peaks centered at the  $2\theta$  values of 18.89, 31.35, 36.76, 38.49, 44.67, 59.28, and 65.23 were well indexed to the planes of (111), (220), (311), (222), (400), (511), and (440) respectively as shown in [Figure 1](#), confirms the cubic and spinel phase of the prepared ZnCo<sub>2</sub>O<sub>4</sub> microstructures belongs to the space group of Fd3m (JCPDS No: 23-1390)<sup>(29)</sup>. Furthermore, some weak diffraction peaks centered at  $2\theta$  values of 31.94, 34.48, 47.66, 62.49, and 66.67° were observed, denoting a significantly less fraction of ZnO in the as-prepared samples formed during the synthesis<sup>(30)</sup>.

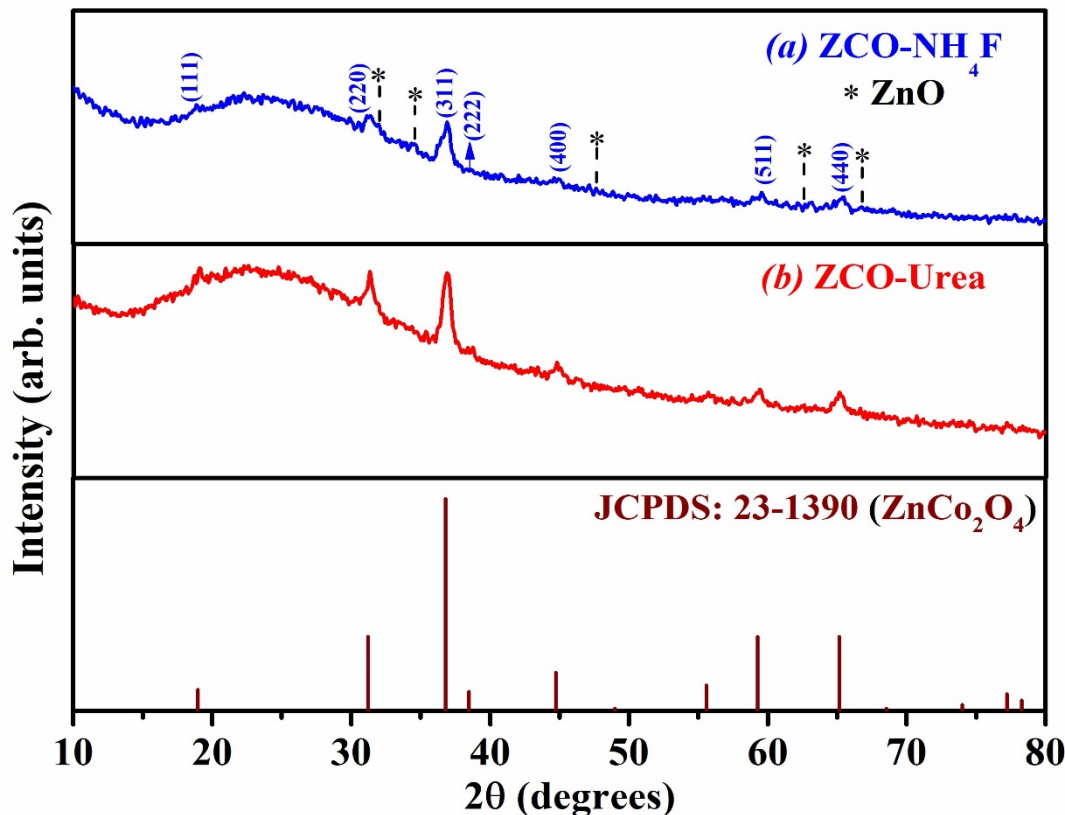


Fig 1. X-ray diffraction (XRD) pattern of ZCO-NH<sub>4</sub>F (a) and ZCO-Urea (b)

The XRD details of the as-prepared materials were analyzed, compared with the standard data, and shown in Table 1.

Table 1. Obtained XRD data for ZCO-Urea and ZCO-NH<sub>4</sub>F

h k l	2θ (°)			d-spacing (Å)			JCPDS No.	Composition
	Standard value	Observed value		Standard value	Observed value			
		ZCO-Urea	ZCO- NH <sub>4</sub> F		ZCO-Urea	ZCO- NH <sub>4</sub> F		
111	18.96	19.12	18.89	4.68	4.53	4.81	23-1390	ZnCo <sub>2</sub> O <sub>4</sub>
220	31.21	31.30	31.30	2.86	2.85	2.85		
311	36.80	36.93	36.83	2.44	2.41	2.41		
222	38.48	38.84	38.51	2.34	2.33	2.33		
400	44.74	44.81	44.61	2.02	2.03	2.03		
511	59.28	59.47	59.47	1.55	1.54	1.54		
440	65.14	65.23	65.35	1.43	1.43	1.43		

The lattice parameter (a), microstrain (ε), dislocation density (δ), cell volume (v), and average crystalline size (D) for both ZCO-Urea and ZCO-NH<sub>4</sub>F microstructures were determined using the following formulae for the dominant peak (311) from the XRD data and represented in Table 2<sup>(31,32)</sup>.

$$2d_{hkl} \sin \theta_{hkl} = \lambda \tag{1}$$

$$\frac{1}{d^2} = \frac{h^2 + k^2 + l^2}{a^2} \tag{2}$$

$$\text{microstrain}(\varepsilon) = \frac{H \cos \theta}{4} \quad (3)$$

$$\text{dislocation density} (\delta) = \frac{1}{D^2} \quad (4)$$

$$\text{cell volume} (v) = abc \sin \beta \quad (5)$$

$$\text{crystalline size} (D) = \frac{K\lambda}{H \cos \theta} \quad (6)$$

Where K is the shape factor, D is the crystallite size in nm,  $\theta$  is the peak position in  $^\circ$ , H is full width at half maximum in radians, and d is the interplanar distance in  $\text{\AA}$  and h, k, l are the Miller indices and a, b, c,  $\beta$  are the lattice parameters.

**Table 2.** Structural parameters of ZCO-Urea and ZCO-NH<sub>4</sub>F

Physical quantity (symbol) (units)	ZCO-Urea	ZCO- NH <sub>4</sub> F
Lattice parameter (a) ( $\text{\AA}$ )	8.35	9.46
Micro strain ( $\varepsilon$ ) $\times 10^{-3}$	1.56	1.67
Dislocation density ( $\delta$ ) $\times 10^{-15}$	2.11	2.38
Cell volume (v) ( $\approx \text{nm}^3$ )	0.52	0.84
Crystalline size (D) (nm)	21.79	20.49

The sharp and broadened diffraction peaks reveal the poor crystallinity and small crystallite size of the ZCO-NH<sub>4</sub>F that play a vital role in enhancing the electrode material's electrochemical behavior than ZCO-Urea. This enhancement was achieved due to the availability of more transportation channels in a low crystalline material compared to a highly crystalline one<sup>(33,34)</sup>.

### 3.2 FT-IR analysis

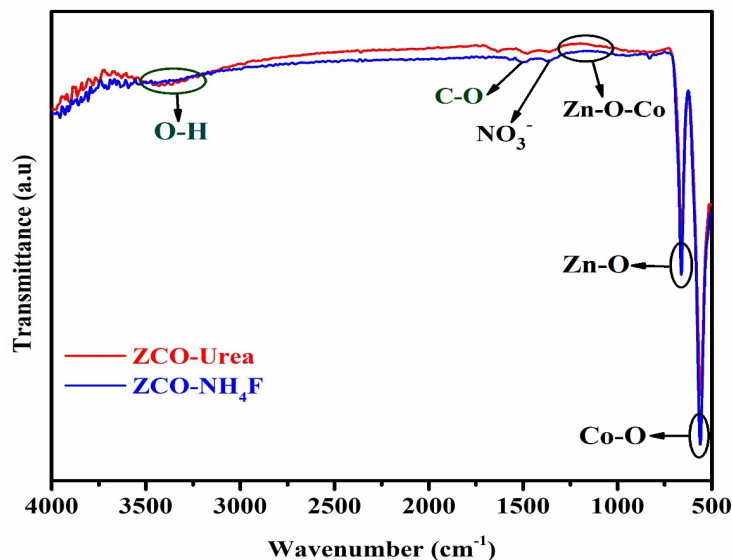


**Fig 2.** FT-IR spectrum of ZCO-Urea and ZCO-NH<sub>4</sub>F

FT-IR spectroscopy is used to identify the major functional groups and chemical species present in the as-prepared ZCO microstructures and presented in Figure 2. The broadband at around  $3360\text{--}3460\text{ cm}^{-1}$  can be attributed to the OH- group's stretching vibrations. The low-intensity band at about  $1477\text{ cm}^{-1}$  can be attributed to the C-O stretching vibration. The peak observed at around  $1385\text{ cm}^{-1}$  represents the presence of  $\text{NO}_3^-$  ions, originated from the precursor medium. The band observed at about  $1105\text{ cm}^{-1}$  confirms the formation of the Zn-O-Co bond. The sharp peaks observed at  $665$  and  $564\text{ cm}^{-1}$  represent the presence of Zn-O and Co-O stretching vibrations, respectively, for both the samples<sup>(35–37)</sup>.

### 3.3 Morphological analysis

The surface morphology and structural features of the ZCO samples were analyzed through FE-SEM analysis. The ZCO-Urea sample exhibits rod-like microstructures (Figure 3 (a)) with in homogeneous aspect ratios having an average length of several micrometres whose surface comprises several agglomerated nanoparticles. Further, when the urea is replaced by ammonium fluoride ( $\text{NH}_4\text{F}$ ), the ZCO sample exhibit hexagonal-shaped microstructures. These microstructures are uniform-sized and consist of numerous irregular micropores formed during the sample's annealing treatment. The high aspect ratio and surface to volume ratios, and high porosity of uniformly distributed hexagonal microstructures provide more surface area to access the electrolyte, increasing the number of electroactive sites resulting in better charge transfer kinetics that leads to the improved electrochemical performance<sup>(38)</sup>.

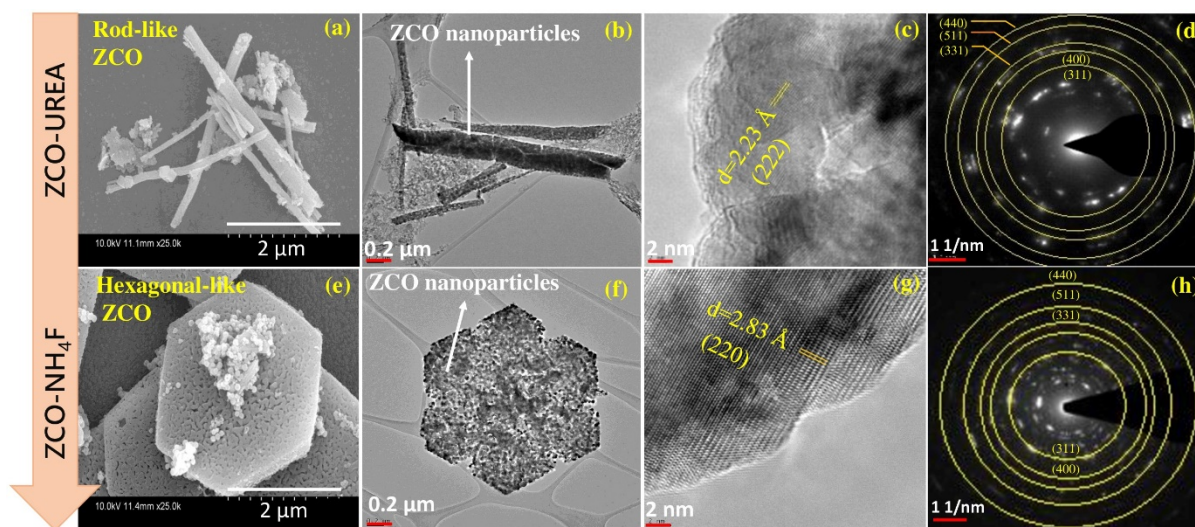


Fig 3. SEM (a, e), TEM (b, c, f, g) images and SAED pattern (d, h) of ZCO-Urea and ZCO-NH<sub>4</sub>F, respectively

TEM and High-Resolution TEM analyses were carried out for the detailed evaluation of morphology for both rod-like and hexagonal-like structures of the as-prepared ZCO samples. From the TEM images (Figure 3(b, f)), it can be observed that a lot of ZCO nanoparticles aggregated to form rod-like microstructures, whereas most of the pure ZCO nanoparticles piled up to form hexagonal-like microstructures. The interplanar distance (d-spacing) and its corresponding lattice planes of both ZCO-Urea and ZCO-NH<sub>4</sub>F were determined to be  $2.23\text{ \AA}$ ,  $2.83\text{ \AA}$ , respectively, from the HR-TEM image. The porous nature of the hexagonal microstructures can be observed from the TEM analysis, inconsistent with the SEM analysis. The microstructures' porosity provides a more specific surface area and shortens the ion diffusion paths between the electrolyte and active material of the electrode. This improves the number of redox electroactive sites and their utilization ability, which leads to the enhanced electrochemical performance of the hexagonal-like microstructures of the ZCO sample. The selected area electron diffraction (SAED) pattern of both ZCO-Urea and ZCO-NH<sub>4</sub>F samples exhibit regular diffraction fringes as shown in Figure 3(d) and (h) represent the polycrystalline nature of the as-prepared samples which is consistent with the XRD analysis<sup>(39,40)</sup>.

### 3.4 Mechanism

Surfactants play a crucial role in obtaining various microstructures. Growth process of nanomaterials occur in three main stages: nucleation, coalescence, and island formation. During hydrothermal treatment, the process of nucleation begins. After that, in the coalescence stage, small particles start to coagulate, which leads to the aggregation of particles. At this stage, surfactants

are used to control the aggregation rate and initiate morphological changes on the material's surface. During the process of nanoparticle synthesis, surfactants can be assembled into various forms such as monolayer micelles, spherical micelles, rod-like micelles, reverse micelles, and vesicle formation with single/multi-component<sup>(41)</sup>. A layer of H<sub>2</sub>O surrounds the inorganic material of the precursor, and both particles and water droplets are attached with a single/multilayer surfactant. This leads to the formation of different morphological microstructures<sup>(42)</sup>.

In this study, urea is used as a forced hydrolysis agent because of its water solubility at 80 to 100 °C, then gradually decomposes into NH<sub>3</sub> and CO<sub>2</sub><sup>(43)</sup>. Also, NH<sub>3</sub> reacts with water to give NH<sub>4</sub><sup>+</sup> and OH<sup>-</sup>. In the process of oxide crystal growth, fine crystal nuclei are formed. The nanoparticles of this oxide are precipitated due to the increase in pH by NH<sub>4</sub><sup>+</sup> ions generated from NH<sub>3</sub> from the decomposition of urea with increasing temperature. Hydrolysis of urea raises the pH due to the increased release of NH<sub>4</sub><sup>+</sup> from the solution. Under milder conditions and lower urea content, urea hydrolysis proceeds slowly, and primary solutions undergo supersaturation of metal hydroxide species. Thus, the formation of metal-hydroxide crystals occurs by the nucleation process in the crystal's desired growth direction. In addition, increasing the hydrothermal system's pressure and the formation of gas molecules disrupted the growth of crystals, leading to the formation of rod-like morphology<sup>(44,45)</sup>.

Since NH<sub>4</sub>F is an acidic mineralizing agent, it has been used so far to increase the crystallinity and crystal size of various materials grown in the solution method<sup>(46,47)</sup>. In this study, the highly ordered hexagonal-like ZCO microstructure was obtained with the addition of NH<sub>4</sub>F as shown in Figure 3(e, f). NH<sub>4</sub>F can dissociate into NH<sub>4</sub><sup>+</sup> and F<sup>-</sup> ions in precursor solutions and further increase the precursor's solubility and the chemical potential of the solution through F<sup>-</sup>, which is more favorable for microstructure growth. Strong coordination of F<sup>-</sup> ions with metal cations (Zn<sup>2+</sup> and Co<sup>2+</sup>) reduce the rate of release of metal ions and further slows the nucleation rate of ZnCo<sub>2</sub>O<sub>4</sub> precursors resulting in the aggregation of particles to the hexagonal-like morphology. F<sup>-</sup> ion can improve ions' mobility by reducing the solution's viscosity<sup>(48–50)</sup>.

### 3.5 Electrochemical analysis

The electrochemical performance of as-prepared electrodes was evaluated to explore the advantages of the morphologies for the application of supercapacitors. The cyclic voltammetry (CV), chronopotentiometry (GCD), and electrochemical impedance spectroscopy (EIS) measurements were conducted using a three-electrode system with 1 M KOH as electrolyte solution at room temperature. Figure 4 (a), (b) shows the obtained CV curves of ZCO-Urea and ZCO-NH<sub>4</sub>F samples, respectively, within the potential window of 0–0.6 V at different scan rates from 5 to 100 mV s<sup>-1</sup>. A pair of reduction and oxidation peaks are observed for all the CV curves representing the materials' pseudocapacitive nature. For this, a couple of reduction and oxidation peaks are identified at 0.45 V and 0.49 V for ZCO-Urea microstructures and 0.39 V and 0.48 V for ZCO-NH<sub>4</sub>F microstructures respectively for the scan rate of 5 mV s<sup>-1</sup>. The ZCO-NH<sub>4</sub>F electrode possesses a larger integral part surrounded by the CV curve and higher redox current density than that of the ZCO-Urea electrode. It represents the superior super capacitive performance of the ZCO-NH<sub>4</sub>F electrode (Figure 4(c)).

Moreover, the oxidation and reduction peaks shift towards higher and lower potentials as the scan rate increases from 5 to 100 mV s<sup>-1</sup>, indicating the reaction kinetics are reversible during the redox process due to the internal resistance polarization effect of the electrodes. The electrochemical reaction mechanism can be explained with the diffusion of OH<sup>-</sup> ions into the electrode in 1M KOH electrolyte. The corresponding chemical equations associated with the faradaic redox reactions are represented as follows<sup>(51,52)</sup>.



Furthermore, to explain the process associated with the electrodes' electrochemical reactions, the relationship between the peak current and its corresponding square root of the scan rates is studied using the power law<sup>(22)</sup>.

$$i = av^b \quad (9)$$

Where *i*, *v* are peak current and scan rates, respectively. The *a*, *b* are the appropriate constants. The value of the constants can determine the charge storage mechanism present in the reaction. If *b* = 0.5, represents the diffusion-controlled nature of the electrochemical process and if *b* = 1, represents the non-diffusion-controlled surface redox process<sup>(22)</sup>.

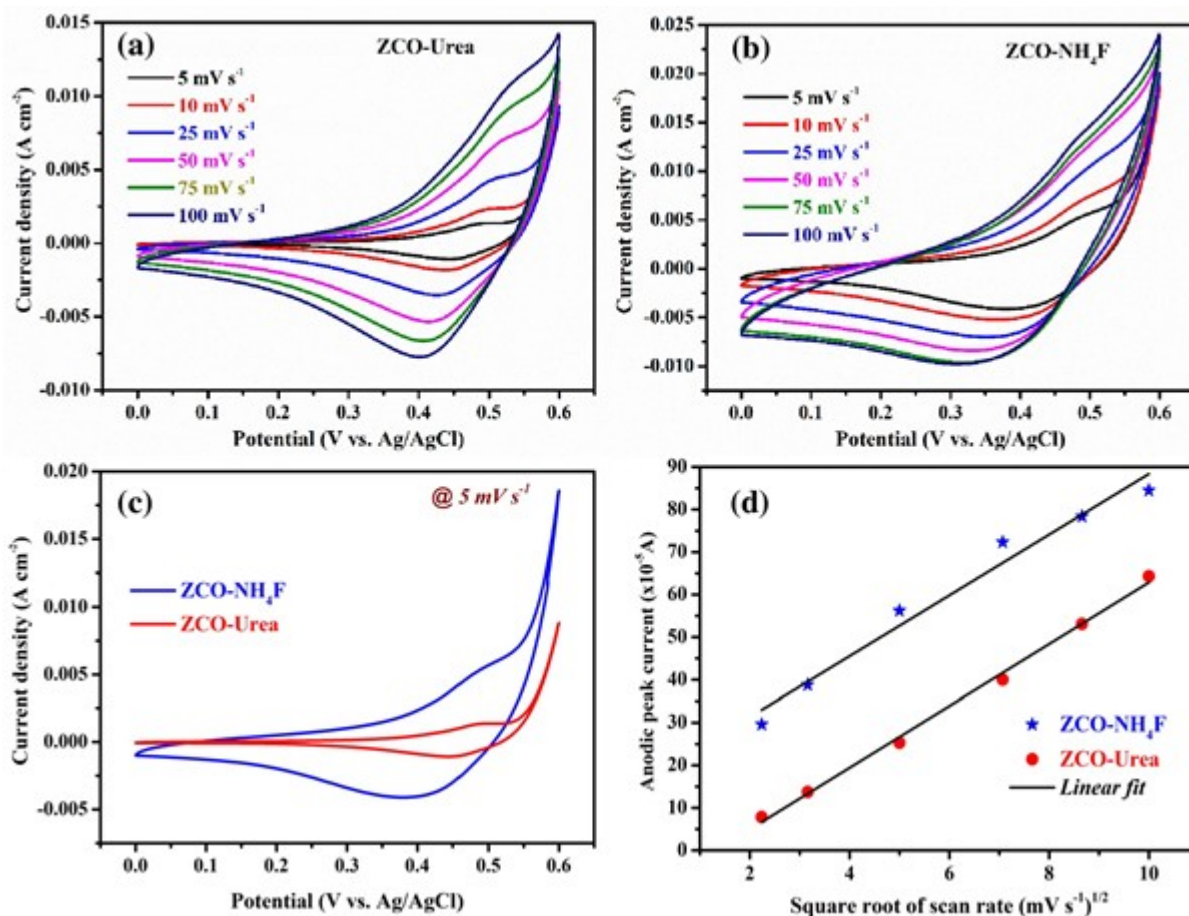


**Fig 4.** Cyclic voltammetry (CV) curves of ZCO-Urea (a) and ZCO-NH<sub>4</sub>F (b) Comparison of CV curves obtained at the scan rate of 5 mV s<sup>-1</sup> (c), Anodic peak current vs. square root of corresponding scan rate plots of both ZCO-Urea and ZCO-NH<sub>4</sub>F microstructures (d)

The anodic peaks of ZCO-Urea and ZCO-NH<sub>4</sub>F electrodes in Figure 4 (d) have b values of 0.54, 0.58 respectively. Since these values are very close to 0.5, it confirms the diffusion-controlled electrochemical process of both electrodes. It is further evidenced by the linearity between the anodic peak current and the square root of their corresponding scan rates and the increase in the integral area surrounded by the cv curves with increasing scan rates<sup>(53)</sup>. Further, the higher current responses of the ZCO-NH<sub>4</sub>F electrode can be observed from the diffusion-controlled process plot compared to the ZCO-Urea electrode, which represents that the ZCO-NH<sub>4</sub>F electrode possesses an excellent electrochemical performance<sup>(54)</sup>. The GCD measurements were carried out to further evaluate the electrodes' electrochemical characteristics in the potential range of 0-0.4 V at various current densities of 10 to 1,000  $\mu\text{A cm}^{-2}$ .

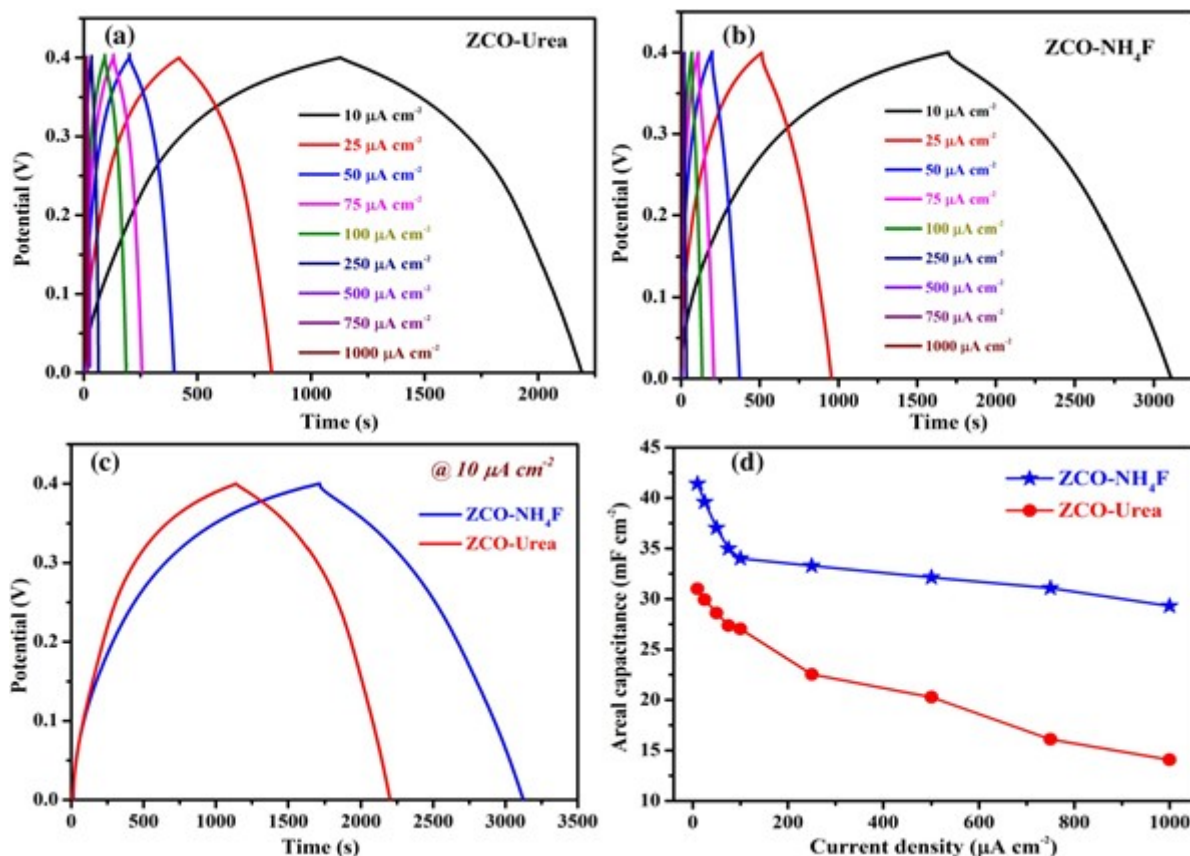


**Fig 5.** Galvanostatic charge-discharge (GCD) curves of ZCO-Urea (a) and ZCO-NH<sub>4</sub>F (b). Comparison of GCD curves obtained at the current density of 10  $\mu\text{A cm}^{-2}$  (c) and variation of calculated areal capacitance values of both ZCO-Urea and ZCO-NH<sub>4</sub>F as a function of various current densities (d)

The highly symmetric and non-linear GCD curves as shown in Figure 5 (a), (b) represent the fast-faradaic redox reactions that occurred at the interface of the electrode/electrolyte and ideal pseudocapacitive behavior, which is inconsistent with the CV analysis<sup>(55)</sup>. The ZCO-Urea and ZCO-NH<sub>4</sub>F samples' areal capacitance is calculated using the following formula<sup>(56)</sup>.

$$C_s = \frac{I \times \Delta t}{S \times \Delta V}$$

Where  $I$  is the discharging current in Amperes,  $\Delta t$  is the discharging time in seconds,  $S$  is the area of the glassy carbon electrode in  $\text{cm}^2$ , and  $\Delta V$  is the potential drop during discharge in volts. An areal capacitance of 31.00, 29.94, 28.62, 27.37, 27.04, 22.54, 20.28, 16.11 and 14.08  $\text{mF cm}^{-2}$  for ZCO-Urea and 41.43, 39.61, 37.04, 34.99, 34.02, 33.29, 32.14, 31.08 and 29.31  $\text{mF cm}^{-2}$  for ZCO-NH<sub>4</sub>F samples was obtained at the current densities of 10, 25, 50, 75, 100, 250, 500, 750 and 1000  $\mu\text{A cm}^{-2}$  respectively. The variation in the electrodes' areal capacitance with respect to the current density was represented in Figure 5(d). The decrease in the areal capacitance with an increase in the current densities is observed and can be attributed to the internal resistance, polarization of the electrodes, and the mechanical stress produced due to the insertion and removal of the electrolyte ions<sup>(29,57)</sup>. Further, a rate capability of 45.4% and 70.7% of initial capacitance was retained even when the current density increased from 10 to 1000  $\mu\text{A cm}^{-2}$  for ZCO-Urea and ZCO-NH<sub>4</sub>F samples respectively. The areal capacitance of the two electrodes of the present work is compared with different transition metal oxides and their combinations and represented in Table 3. From the comparison, one can suggest them for the application of electrode material for supercapacitors.

The cyclic stability test was further used to investigate the supercapacitor performance of the electrodes. Figure 5(a) and (b) represents the cyclic stability of ZCO-Urea and ZCO-NH<sub>4</sub>F samples for 1,000 continuous charge-discharge cycles at a constant current density of 500  $\mu\text{A cm}^{-2}$  in the potential range of 0-0.4 V. Impressively, 156.1% and 150.7% of initial areal capacitance were

**Table 3.** The areal capacitance of different metal oxides in comparison with present work

Different metal oxides and combinations	Synthesis method	Areal capacitance	Ref.
2D-LiCoO <sub>2</sub>	Electrochemical deposition	310 mF cm <sup>-2</sup> @ 5 mV s <sup>-1</sup>	(58)
Hexagonal-like ZnCo <sub>2</sub> O <sub>4</sub>	Hydrothermal	41.43 mF cm <sup>-2</sup> @ 10 μA cm <sup>-2</sup>	Present
NiCo <sub>2</sub> O <sub>4</sub>	Sol-gel method	40.6 mF cm <sup>-2</sup> @ 0.133 mA cm <sup>-2</sup>	(59)
Rod-like ZnCo <sub>2</sub> O <sub>4</sub>	Hydrothermal	31.00 mF cm <sup>-2</sup> @ 10 μA cm <sup>-2</sup>	Present
TiO <sub>2</sub>	Electrochemical anodization	23.24 mF cm <sup>-2</sup> @ 2 mV s <sup>-1</sup>	(60)
Co(OH) <sub>2</sub> /Ni	Electrochemical deposition	22.9 mF cm <sup>-2</sup> @ 5 mV s <sup>-1</sup>	(61)
MnO <sub>2</sub> /MoS <sub>2</sub>	Magnetron sputtering	22.4 mF cm <sup>-2</sup> @ 0.1 mA cm <sup>-2</sup>	(62)
sheet-like ZnCo <sub>2</sub> O <sub>4</sub>	Hydrothermal	16.13 mF cm <sup>-2</sup> @ 10 μA cm <sup>-2</sup>	(56)

retained for ZCO-Urea and ZCO-NH<sub>4</sub>F samples respectively, after cycling for 1,000 cycles indicates the outstanding cycling stability of the as-prepared electrodes.

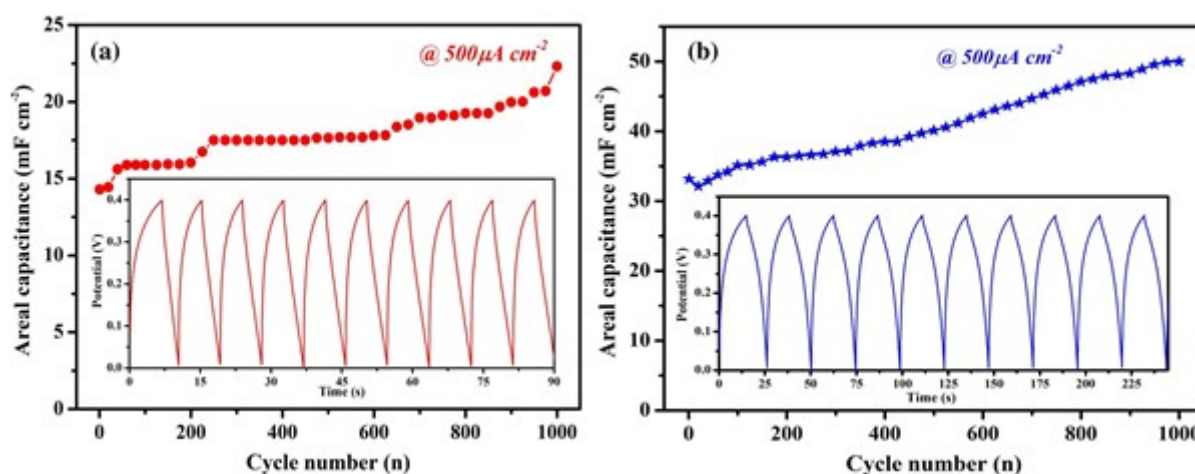


**Fig 6.** Cycling performance of ZCO-Urea (a) and ZCO-NH<sub>4</sub>F (b) for 1,000 continuous charge-discharge cycles. (Insets of (a) and (b) represents GCD curves of the first ten cycles of ZCO-Urea and ZCO-NH<sub>4</sub>F, respectively).

The increase in the electrodes' areal capacitance after cycling is due to the full activation of the electrode material. This activation occurs due to the slow insertion of the electrolyte solution into the bulk structure of the active material and the diffusion of more ions that create a more significant number of electroactive sites within the electrode material<sup>(63)</sup>. A high symmetric nature in the shape of the GCD curves for the first ten charge-discharge cycles was observed for both ZCO-Urea and ZCO-NH<sub>4</sub>F, as shown in the insets of Figure 6 (a) and (b), represents the superior reversible redox behavior of the electrodes<sup>(29)</sup>.

To further study the two electrodes' electrochemical behavior, EIS was performed before and after conducting the cycling stability test within the frequency range of 0.001 Hz to 100 kHz at an open circuit potential with an AC perturbation of 5 mV amplitude. All the Nyquist plots exhibit a straight line in the low-frequency section and a semi-circle in the high-frequency area represented in Figure 7 (a) and (b).

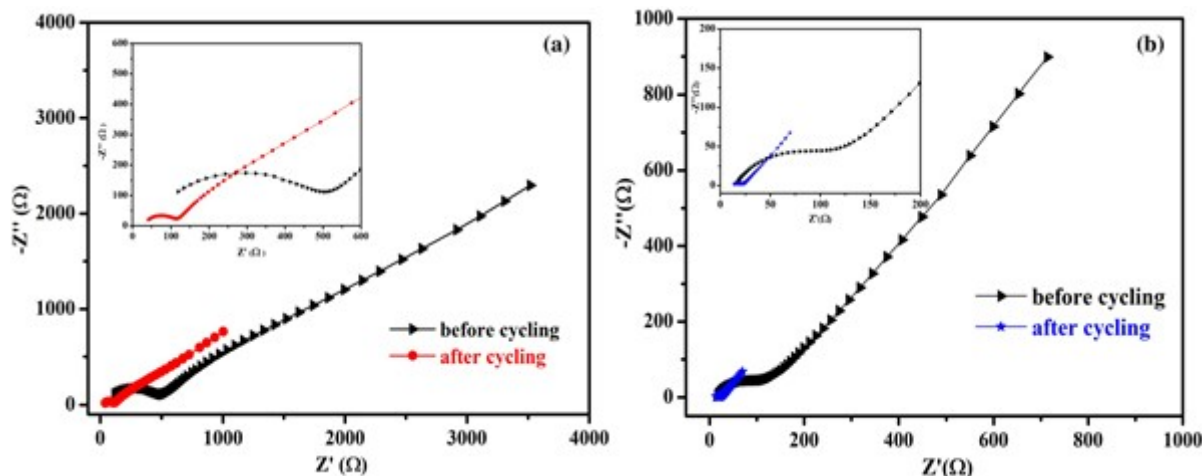


**Fig 7.** Nyquist plots of ZCO-Urea (a) and ZCO-NH<sub>4</sub>F (b) before and after cycling for 1000 cycles. (Inset shows the magnified images of Nyquist plots of ZCO-Urea and ZCO-NH<sub>4</sub>F, respectively).

Firstly, the internal resistance ( $R_s$ ), which includes the electrolyte resistance, electrode resistance, and contact resistance at the electrode/electrolyte interface of the electrochemical system, was estimated at the intercept of the high-frequency region with the real axis. The  $R_s$  values are measured for both ZCO-Urea and ZCO-NH<sub>4</sub>F samples are shown in Table 4. The ZCO-NH<sub>4</sub>F electrode's  $R_s$  is lower than the ZCO-Urea electrode, indicating its good rate capability<sup>(64,65)</sup>. Secondly, the slope of the linear part of the Nyquist diagrams at the low-frequency region represents the Warburg impedance ( $W$ ), associated with the ion's diffusion of electrolyte into the electrode surface. The lower slope of the straight line for both ZCO-Urea and ZCO-NH<sub>4</sub>F samples after cycling indicates a gradual decrement in ion transfer rates between electrode and electrolyte that helps in utilizing more active material. However, the ZCO-NH<sub>4</sub>F electrode shown less Warburg impedance represents its greater ions diffusion of electrolyte with the electrode surface than the ZCO-Urea electrode. Thirdly, the diameter semi-circle in the high-frequency section represents interfacial charge transfer resistance ( $R_{ct}$ ) associated with the faradaic reactions. The decrease in the semi-circle diameter is observed after cycling in both the electrodes indicating their improved electronic conductivity (Table 4).

**Table 4.** Series resistance ( $R_s$ ) and charge transfer resistance ( $R_{ct}$ ) of ZCO-Urea and ZCO-NH<sub>4</sub>F before and after cycling.

Resistance	ZCO-Urea		ZCO-NH <sub>4</sub> F	
	Before cycling	After cycling	Before cycling	After cycling
$R_s$ (Ω)	473	39.8	16.9	13.7
$R_{ct}$ (Ω)	134.5	82.9	128.6	82.4

However, the lowest  $R_{ct}$  of the ZCO-NH<sub>4</sub>F electrode shows its improved electronic conductivity than the ZCO-Urea electrode. The decrease in  $R_{ct}$  after cycling can be attributed to sufficient electrolyte penetration and wetting within the electrode's interior that helps for the rapid transportation of electrons, thus enhancing the electronic conductivity. These results conclude that the ZCO-NH<sub>4</sub>F electrode, after cycling with desirable properties like fast ion transport rates and charge transfer kinetics shows excellent electrochemical properties<sup>(36,66,67)</sup>.

## 4 Conclusions

The hexagonal/rod-shaped ZCO microstructures were synthesized by replacing the surfactant in the reaction by a simple hydrothermal method followed by further annealing. The structural characteristics and morphology were assessed by XRD, FE-SEM, HR-TEM, and SAED analyses. ZCO's two different microstructures were evaluated as electrode materials for supercapacitors through electrochemical studies such as CV, GCD, and EIS. A high areal capacitance (41.43 mF cm<sup>-2</sup> for ZCO-NH<sub>4</sub>F and 31.00 mF cm<sup>-2</sup> for ZCO-Urea at 10 μA cm<sup>-2</sup>) and superior cycling stability (150.7% for ZCO-NH<sub>4</sub>F, 156.1% for ZCO-Urea of initial capacitance retained after 1,000 cycles) and good rate capability (70.7% for ZCO-NH<sub>4</sub>F, 45.4% for ZCO-Urea when the current density was increased from 10 μA cm<sup>-2</sup> to 1,000 μA cm<sup>-2</sup>) were obtained for both the electrodes. The unique hierarchical architectures with porous material nature helped in obtaining the results mentioned above.

## Acknowledgements

The author K. Prasad is highly thankful to UGC, Govt. of India for providing financial assistance in the form of Rajiv Gandhi National Fellowship (RGNF) for pursuing a Ph.D. programme.

## References

- Sun A, Xie L, Wang D, Wu Z. Enhanced energy storage performance from Co-decorated MoS<sub>2</sub> nanosheets as supercapacitor electrode materials. *Ceramic International*. 2018;44:13434–13438. Available from: <https://doi.org/10.1016/j.ceramint.2018.04.113>.
- Kulkarni P, Nataraj SK, Balakrishna RG, Nagaraju DH, Reddy MV. Nanostructured binary and ternary metal sulfides: synthesis methods and their application in energy conversion and storage devices. *J Mater Chem A*. 2017;5(42):22040–22094. Available from: <https://dx.doi.org/10.1039/c7ta07329a>.
- Yi TF, Li Y, Li YM, Luo S, Liu YG. ZnS nanoparticles as the electrode materials for high-performance supercapacitors. *Solid State Ionics*. 2019. Available from: <https://doi.org/10.1016/j.ssi.2019.115074>.
- Reddy BJ, Vickraman P, Justin AS. A facile synthesis of novel a-ZnMoO<sub>4</sub> microspheres as electrode material for supercapacitor applications. *Bulletin of Materials Science*. 2019;42:1–6. Available from: <https://doi.org/10.1007/s12034-019-1749-9>.
- Kazemi SH, Tabibpour M, Kiani MA, Kazemi H. An advanced asymmetric supercapacitor based on a binder-free electrode fabricated from ultrathin CoMoO<sub>4</sub> nano-dandelions. *RSC Advances*. 2016;6(75):71156–71164. Available from: <https://dx.doi.org/10.1039/c6ra05703a>.
- Xu K, Chao J, Li W, Liu Q, Wang Z, Liu X, et al. CoMoO<sub>4</sub>•0.9H<sub>2</sub>O nanorods grown on reduced graphene oxide as advanced electrochemical pseudocapacitor materials. *RSC Advances*. 2014;4:34307–34314. Available from: <https://doi.org/10.1039/c4ra04827j>.
- Mandal M, Ghosh D, Giri S, Shakir I, Das CK. Polyaniline-wrapped 1D CoMoO<sub>4</sub>•0.75H<sub>2</sub>O nanorods as electrode materials for supercapacitor energy storage applications. *RSC Advances*. 2014;p. 30832–30839. Available from: <https://doi.org/10.1039/c4ra03399j>.
- Candler J, Elmore T, Gupta BK, Dong L, Palchoudhury S, Gupta RK. New insight into high-temperature driven morphology reliant CoMoO<sub>4</sub> flexible supercapacitors. *New Journal of Chemistry*. 2015;39(8):6108–6116. Available from: <https://dx.doi.org/10.1039/c5nj00446b>.
- Zhu J, Xiang L, Xi D, Zhou Y, Yang J. One-step hydrothermal synthesis of flower-like CoS hierarchitectures for application in supercapacitors. *Bulletin of Materials Science*. 2018;41(2). Available from: <https://dx.doi.org/10.1007/s12034-018-1570-x>.
- Pan Y, Gao H, Zhang M, Li L, Wang Z. Facile synthesis of ZnCo<sub>2</sub>O<sub>4</sub> micro-flowers and micro-sheets on Ni foam for pseudocapacitor electrodes. *Journal of Alloys and Compounds*. 2017;702:381–387. Available from: <https://doi.org/10.1016/j.jallcom.2017.01.136>.
- Cheng M, Fan H, Song Y, Cui Y, Wang R. Interconnected hierarchical NiCo<sub>2</sub>O<sub>4</sub> microspheres as high-performance electrode materials for supercapacitors. *Dalton Transactions*. 2017;46:9201–9209. Available from: <https://doi.org/10.1039/c7dt01289f>.
- Ji Y, Xie J, Wu J, Yang Y, Fu XZ, Sun R, et al. Hierarchical nanothorns MnCo<sub>2</sub>O<sub>4</sub> grown on porous/dense Ni bi-layers coated Cu wire current collectors for high performance flexible solid-state fiber supercapacitors. *Journal of Power Sources*. 2018;393:54–61. Available from: <https://doi.org/10.1016/j.jpowsour.2018.04.109>.
- Guan B, Guo D, Hu L, Zhang G, Fu T, Ren W, et al. Facile synthesis of ZnCo<sub>2</sub>O<sub>4</sub> nanowire cluster arrays on Ni foam for high-performance asymmetric supercapacitors. *J Mater Chem A*. 2014;2(38):16116–16123. Available from: <https://dx.doi.org/10.1039/c4ta02378a>.
- Ensaifi AA, Moosavifard SE, Rezaei B, Kaverlavani SK. Engineering onion-like nanoporous CuCo<sub>2</sub>O<sub>4</sub> hollow spheres derived from bimetal–organic frameworks for high-performance asymmetric supercapacitors. *Journal of Materials Chemistry A*. 2018;6(22):10497–10506. Available from: <https://dx.doi.org/10.1039/c8ta02819b>.
- Raut SS, Sankapal BR. First report on synthesis of ZnFe<sub>2</sub>O<sub>4</sub> thin film using successive ionic layer adsorption and reaction: Approach towards solid-state symmetric supercapacitor device. *Electrochimica Acta*. 2018;273:203–211. Available from: <https://doi.org/10.1016/j.electacta.2016.03.059>.
- Rajesh JA, Min BK, Kim JH, Kim H, Ahn KS. Cubic Spinel AB<sub>2</sub>O<sub>4</sub> Type Porous ZnCo<sub>2</sub>O<sub>4</sub> Microspheres: Facile Hydrothermal Synthesis and Their Electrochemical Performances in Pseudocapacitor. *Journal of The Electrochemical Society*. 2016;163. Available from: <https://doi.org/10.1149/2.0071613jes>.
- Rajesh JA, Min BK, Kim JH, Kang SH, Kim H, Ahn KS. Facile hydrothermal synthesis and electrochemical supercapacitor performance of hierarchical coral-like ZnCo<sub>2</sub>O<sub>4</sub> nanowires. *Journal of Electroanalytical Chemistry*. 2017;785:48–57. Available from: <https://doi.org/10.1016/j.jelechem.2016.12.027>.
- Kathalingam A, Ramesh S, Yadav HM, Choi JH, Kim HS, Kim HS. Nanosheet-like ZnCo<sub>2</sub>O<sub>4</sub>@nitrogen doped graphene oxide/polyaniline composite for supercapacitor application: Effect of polyaniline incorporation. *Journal of Alloys and Compounds*. 2020;830. Available from: <https://dx.doi.org/10.1016/j.jallcom.2020.154734>.
- Yang Y, Yang C, Tao K, Ma Q, Han L. Construction of S-doped ZnCo<sub>2</sub>O<sub>4</sub> microspindles with enhanced electrochemical performance for supercapacitors. *Vacuum*;181. Available from: <https://doi.org/10.1016/j.vacuum.2020.109740>.
- Yu H, Zhao H, Wu Y, Chen B, Sun J. Electrospun ZnCo<sub>2</sub>O<sub>4</sub>/C composite nanofibers with superior electrochemical performance for supercapacitor. *Journal of Physics and Chemistry of Solids*. 2020;140. Available from: <https://doi.org/10.1016/j.jpics.2020.109385>.
- Reddy GR, Dillip GR, Sreekanth TVM, Rajavaram R, Raju BDP, Nagajyothi PC, et al. In situ engineered 0D interconnected network-like CNS decorated on Co-rich ZnCo<sub>2</sub>O<sub>4</sub> 2D nanosheets for high-performance supercapacitors. *Journal of the Taiwan Institute of Chemical Engineers*. 2020;113:155–164. Available from: <https://dx.doi.org/10.1016/j.jtice.2020.08.002>.
- Reddy GR, Kumar NS, Raju BDP, Shanmugam G, Al-Ghurabi EH, Asif M. Enhanced Supercapacitive Performance of Higher-Ordered 3D-Hierarchical Structures of Hydrothermally Obtained ZnCo<sub>2</sub>O<sub>4</sub> for Energy Storage Devices. *Nanomaterials*. 2020;10(6). Available from: <https://dx.doi.org/10.3390/nano10061206>.
- Reddy GR, Dillip GR, Sreekanth TVM, Rajavaram R, Raju BDP, Nagajyothi PC, et al. Mechanistic investigation of defect-engineered, non-stoichiometric, and Morphology-regulated hierarchical rhombus-/spindle-/peanut-like ZnCo<sub>2</sub>O<sub>4</sub> microstructures and their applications toward high-performance supercapacitors. *Applied Surface Science*. 2020;529. Available from: <https://dx.doi.org/10.1016/j.apsusc.2020.147123>.
- Liu M, Chang J, Sun J, Gao L. Synthesis of porous NiO using NaBH<sub>4</sub> dissolved in ethylene glycol as precipitant for high-performance supercapacitor. *Electrochimica Acta*. 2013;107:9–15. Available from: <https://dx.doi.org/10.1016/j.electacta.2013.05.122>.
- Gund GS, Dubal DP, Dhawale DS, Shinde SS, Lokhande CD. Porous CuO nanosheet clusters prepared by a surfactant assisted hydrothermal method for high performance supercapacitors. *RSC Advances*. 2013;3(46). Available from: <https://dx.doi.org/10.1039/c3ra43254h>.
- Barmi MJ, Sundaram MM. Role of polymeric surfactant in the synthesis of cobalt molybdate nanospheres for hybrid capacitor applications. *RSC Advances*. 2016;6(42):36152–36162. Available from: <https://dx.doi.org/10.1039/c6ra02628a>.

- 27) Zhang H, Lu C, Hou H, Ma Y, Yuan S. Facile morphology-controlled synthesis of  $\text{Co}_3\text{O}_4$  nanostructure on carbon cloth and their morphology-dependent pseudocapacitive performances. *Journal of Alloys and Compounds*. 2019;797:970–977. Available from: <https://dx.doi.org/10.1016/j.jallcom.2019.05.206>.
- 28) Acharya J, Ko TH, Seo MK, Khil MS, Kim HY, Kim BS. Oxalic acid assisted rapid synthesis of mesoporous  $\text{NiCo}_2\text{O}_4$  nanorods as electrode materials with higher energy density and cycle stability for high-performance asymmetric hybrid supercapacitor applications. *Journal of Colloid and Interface Sciences*. 2020;564:65–76. Available from: <https://doi.org/10.1016/j.jcis.2019.12.098>.
- 29) Han X, Liao F, Zhang Y, Han X, Xu C, Chen H. Solvothermal preparation of zinc cobaltite mesoporous microspheres for high-performance electrochemical supercapacitors. *Journal of Alloys and Compounds*. 2019;781:425–432. Available from: <https://doi.org/10.1016/j.jallcom.2018.12.079>.
- 30) Lahure P, Salunke P, Soliwal R, Yadav A, Tripathi S, Koser AA. X-Ray Diffraction Study of ZnO Nanoparticles. *International Journal of Scientific Research in Physics and Applied Sciences*. 2015;3:32–33. Available from: [https://www.isroset.org/pub\\_paper/ijsrpas/isroset-nsrtp-2014-0008.pdf](https://www.isroset.org/pub_paper/ijsrpas/isroset-nsrtp-2014-0008.pdf).
- 31) Priya M, Premkumar VK, Vasantharani P, Sivakumar G. Structural and electrochemical properties of  $\text{ZnCo}_2\text{O}_4$  nanoparticles synthesized by hydrothermal method. *Vacuum*. 2019;167:307–312. Available from: <https://dx.doi.org/10.1016/j.vacuum.2019.06.020>.
- 32) Hossen MM, Hossen MB. Structural, electrical and magnetic properties of  $\text{Ni}_{0.5}\text{Cu}_{0.2}\text{Cd}_{0.3}\text{La}_x\text{Fe}_{2-x}\text{O}_4$  nano-ferrites due to lanthanum doping in the place of trivalent iron. *Physica B: Condensed Matter*. 2020;585. Available from: <https://dx.doi.org/10.1016/j.physb.2020.412116>.
- 33) Kianpour G, Salavati-Niasari M, Emadi H. Precipitation synthesis and characterization of cobalt molybdates nanostructures. *Superlattices and Microstructures*. 2013;58:120–129. Available from: <https://dx.doi.org/10.1016/j.spmi.2013.01.014>.
- 34) Liu MC, Kong L, Kang L, Li X, Walsh FC, Xing M, et al. Synthesis and characterization of  $\text{M}_3\text{V}_2\text{O}_8$  (M = Ni or Co) based nanostructures: A new family of high performance pseudocapacitive materials. *Journal of Materials Chemistry A*. 2014;2:4919–4926. Available from: <https://doi.org/10.1039/c4ta00582a>.
- 35) Shang Y, Xie T, Gai Y, Su L, Gong L, Lv H. Electrochimica Acta Self-assembled hierarchical peony-like  $\text{ZnCo}_2\text{O}_4$  for high-performance asymmetric supercapacitors. *Electrochimica Acta*. 2017;253:281–290. Available from: <https://doi.org/10.1016/j.electacta.2017.09.042>.
- 36) Mary AJC, Bose AC. Surfactant assisted  $\text{ZnCo}_2\text{O}_4$  nanomaterial for supercapacitor application. *Applied Surface Science*. 2018;449:105–112. Available from: <https://dx.doi.org/10.1016/j.apsusc.2018.01.117>.
- 37) Raut SS, Sankapal BR. Porous zinc cobaltite ( $\text{ZnCo}_2\text{O}_4$ ) film by successive ionic layer adsorption and reaction towards solid-state symmetric supercapacitive device. *Journal of Colloid and Interface Science*. 2017;487:201–208. Available from: <https://dx.doi.org/10.1016/j.jcis.2016.10.025>.
- 38) Venkatachalam V, Alsalmeh A, Alghamdi A, Jayavel R. Hexagonal-like  $\text{NiCo}_2\text{O}_4$  nanostructure based high-performance supercapacitor electrodes. *Ionics*. 2017;23(4):977–984. Available from: <https://dx.doi.org/10.1007/s11581-016-1868-x>.
- 39) Bhagwan J, Nagaraju G, Ramulu B, Yu JS. Promotive Effect of MWCNT on  $\text{ZnCo}_2\text{O}_4$  Hexagonal Plates and Their Application in Aqueous Asymmetric Supercapacitor. *Journal of The Electrochemical Society*. 2019;166(2):A217–A224. Available from: <https://dx.doi.org/10.1149/2.0631902jes>.
- 40) Xiao X, Wang G, Zhang M, Wang Z, Zhao R, Wang Y. Electrochemical performance of mesoporous  $\text{ZnCo}_2\text{O}_4$  nanosheets as an electrode material for supercapacitor. *Ionics (Kiel)*. 2018;24:2435–2443. Available from: <https://doi.org/10.1007/s11581-017-2354-9>.
- 41) Dixit SG, Mahadeshwar AR, Haram SK. Some aspects of the role of surfactants in the formation of nanoparticles. *Colloids and Surfaces A: Physicochemical and Engineering Aspects*. 1998;133(1-2):69–75. Available from: [https://dx.doi.org/10.1016/S0927-7757\(97\)00126-x](https://dx.doi.org/10.1016/S0927-7757(97)00126-x).
- 42) Morsy SMI. Role of surfactants in nanotechnology and their applications. *International Journal of Current Microbiology and Applied Sciences*. 2014;3:237–260. Available from: <https://www.ijcmas.com/vol-3-5/salwa%20m.i.%20morsy.pdf>.
- 43) Hu MZC, Harris MT, Byers CH. Nucleation and growth for synthesis of nanometric zirconia particles by forced hydrolysis. *Journal of Colloid and Interface Sciences*. 0198;198:87–99. Available from: <https://doi.org/10.1006/jcis.1997.5290>.
- 44) Kakiuchi K, Hosono E, Kimura T, Imai H, Fujihara S. Fabrication of mesoporous ZnO nanosheets from precursor templates grown in aqueous solutions. *Journal of Sol-Gel Science and Technology*. 2006;39(1):63–72. Available from: <https://dx.doi.org/10.1007/s10971-006-6321-6>.
- 45) Marinho JZ, Romeiro FC, Lemos SCS, Motta FV, Riccardi CS, Li MS, et al. Urea-Based Synthesis of Zinc Oxide Nanostructures at Low Temperature. *Journal of Nanomaterials*. 2012;2012:1–7. Available from: <https://dx.doi.org/10.1155/2012/427172>.
- 46) Caullet P, Paillaud JL, Simon-Masseron A, Souillard M, Patarin J. The fluoride route: a strategy to crystalline porous materials. *Comptes Rendus Chimie*. 2005;8(3-4):245–266. Available from: <https://dx.doi.org/10.1016/j.crci.2005.02.001>.
- 47) Chen G, Jiang L, Wang L, Zhang J. Synthesis of mesoporous ZSM-5 by one-pot method in the presence of polyethylene glycol. *Microporous and Mesoporous Materials*. 2010;134:189–194. Available from: <https://doi.org/10.1016/j.micromeso.2010.05.025>.
- 48) Du H, Wang Y, Yuan H, Jiao L. Facile Synthesis and High Capacitive Performance of 3D Hierarchical  $\text{Ni}(\text{OH})_2$  Microspheres. *Electrochimica Acta*. 0196;196:84–91. Available from: <https://doi.org/10.1016/j.electacta.2016.02.190>.
- 49) Wu X, Han X, Ma X, Zhang W, Deng Y, Zhong C, et al. Morphology-Controllable Synthesis of Zn-Co-Mixed Sulfide Nanostructures on Carbon Fiber Paper Toward Efficient Rechargeable Zinc-Air Batteries and Water Electrolysis. *ACS Applied Materials and Interfaces*. 2017;9:12574–12583. Available from: <https://doi.org/10.1021/acsami.6b16602>.
- 50) Wang Z, Lu Y, Yuan S, Shi L, Zhao Y, Zhang M, et al. Hydrothermal synthesis and humidity sensing properties of size-controlled Zirconium Oxide ( $\text{ZrO}_2$ ) nanorods. *Journal of Colloid and Interface Sciences*. 2013;396:9–15. Available from: <https://doi.org/10.1016/j.jcis.2012.12.068>.
- 51) Wu C, Cai J, Zhang Q, Zhou X, Zhu Y, Li L, et al. Direct growth of urchin-like  $\text{ZnCo}_2\text{O}_4$  microspheres assembled from nanowires on nickel foam as high-performance electrodes for supercapacitors. *Electrochimica Acta*. 2015;169:202–209. Available from: <https://doi.org/10.1016/j.electacta.2015.04.079>.
- 52) Jadhav HS, Roy A, Chung WJ, Seo JG. Growth of urchin-like  $\text{ZnCo}_2\text{O}_4$  microspheres on nickel foam as a binder-free electrode for high-performance supercapacitor and methanol electro-oxidation. *Electrochimica Acta*. 2017;246:941–950. Available from: <https://dx.doi.org/10.1016/j.electacta.2017.06.118>.
- 53) Song D, Zhu J, Li J, Pu T, Huang B, Zhao C, et al. Free-standing Two-dimensional Mesoporous  $\text{ZnCo}_2\text{O}_4$  Thin Sheets Consisting of 3D Ultrathin Nanoflake Array Frameworks for High Performance Asymmetric Supercapacitor. *Electrochimica Acta*. 2017;257:455–464. Available from: <https://dx.doi.org/10.1016/j.electacta.2017.10.116>.
- 54) Gutturu RR, M STV, Rajavaram R, Borelli DPR, Dillip GR, Nagajyothi PC, et al. Effect of reaction time and PVP contents on morphologies of hierarchical 3D flower-like  $\text{ZnCo}_2\text{O}_4$  microstructures for energy storage devices. *International Journal of Energy Research*. 2020;p. 1–15. Available from: <https://doi.org/10.1002/er.5719>.
- 55) Cheng J, Lu Y, Qiu K, Yan H, Hou X, Xu J, et al. Mesoporous  $\text{ZnCo}_2\text{O}_4$  nanoflakes grown on nickel foam as electrodes for high performance supercapacitors. *Physical Chemistry and Chemical Physics*. 2015;17:17016–17022. Available from: <https://doi.org/10.1039/c5cp01629k>.
- 56) Prasad K, Reddy GR, Rajesh M, Babu PR, Shanmugam G, Sushma NJ, et al. Electrochemical Performance of 2D-Hierarchical sheet-like  $\text{ZnCo}_2\text{O}_4$  Microstructures for Supercapacitor Applications. *Crystals*. 2020;10:1–13. Available from: <https://doi.org/10.3390/cryst10070566>.
- 57) Wang X, Li W, Wang X, Zhang J, Sun L, Gao C, et al. Electrochemical properties of  $\text{NiCo}_2\text{O}_4$  synthesized by hydrothermal method. *RSC Advances*. 2017;7:50753–50759. Available from: <https://doi.org/10.1039/c7ra10232a>.

- 58) Lu J, Ran H, Li J, Wan J, Wang C, Ji P, et al. A fast composite-hydroxide-mediated approach for synthesis of 2D-LiCoO<sub>2</sub> for high performance asymmetric supercapacitor. *Electrochimica Acta*. 2020;331. Available from: <https://doi.org/10.1016/j.electacta.2019.135426>.
- 59) Liu Y, Wang N, Yang C, Hu W. Sol-gel synthesis of nanoporous NiCo<sub>2</sub>O<sub>4</sub> thin films on ITO glass as high-performance supercapacitor electrodes. *Ceramics International*. 2016;42:11411–11416. Available from: <https://doi.org/10.1016/j.ceramint.2016.04.071>.
- 60) Zhang J, Wang Y, Wu J, Shu X, Yu C, Cui J, et al. Remarkable supercapacitive performance of TiO<sub>2</sub> nanotube arrays by introduction of oxygen vacancies. *Chemical Engineering Journal*. 2017;313:1071–1081. Available from: <https://doi.org/10.1016/j.cej.2016.11.004>.
- 61) Soram BS, Dai J, Kshetri T, Kim NH, Lee JH. Vertically grown and intertwined Co(OH)<sub>2</sub> nanosheet@Ni-mesh network for transparent flexible supercapacitor. *Chemical Engineering Journal*. 2020;391. Available from: <https://dx.doi.org/10.1016/j.cej.2019.123540>.
- 62) Zhang H, Wei J, Yan Y, Guo Q, Xie L, Yang Z, et al. Facile and scalable fabrication of MnO<sub>2</sub> nanocrystallines and enhanced electrochemical performance of MnO<sub>2</sub>/MoS<sub>2</sub> inner heterojunction structure for supercapacitor application. *Journal of Power Sources*. 2020. Available from: <https://doi.org/10.1016/j.jpowsour.2019.227616>.
- 63) Liu XY, Zhang YQ, Xia XH, Shi SJ, Lu Y, Wang XL, et al. Self-assembled porous NiCo<sub>2</sub>O<sub>4</sub> hetero-structure array for electrochemical capacitor. *Journal of Power Sources*. 2013;239:157–163. Available from: <https://doi.org/10.1016/j.jpowsour.2013.03.106>.
- 64) Yang W, Gao Z, Ma J, Wang J, Wang B, Liu L. Effects of solvent on the morphology of nanostructured Co<sub>3</sub>O<sub>4</sub> and its application for high-performance supercapacitors. *Electrochimica Acta*. 2013;112:378–385. Available from: <https://doi.org/10.1016/j.electacta.2013.08.056>.
- 65) Ding R, Gao H, Zhang M, Zhang J, Zhang X. Controllable synthesis of Ni<sub>3-x</sub>Co<sub>x</sub>S<sub>4</sub> nanotube arrays with different aspect ratios grown on carbon cloth for high-capacity supercapacitors. *RSC Advances*. 2015;5:48631–48637. Available from: <https://doi.org/10.1039/c5ra06440f>.
- 66) Liu MC, Kong L, Lu C, Li XM, Luo YC, Kang L. Facile fabrication of CoMoO<sub>4</sub> nanorods as electrode material for electrochemical capacitors. *Materials Letters*. 2013;94:197–200. Available from: <https://doi.org/10.1016/j.matlet.2012.12.057>.
- 67) Fu W, Wang Y, Han W, Zhang Z, Zha H, Xie E. Construction of hierarchical ZnCo<sub>2</sub>O<sub>4</sub>@Ni<sub>x</sub>Co<sub>2-x</sub>(OH)<sub>6-x</sub> core/shell nanowire arrays for high-performance supercapacitors. *Journal of Materials Chemistry A*. 2016;4:173–182. Available from: <https://doi.org/10.1039/c5ta07965a>.